

Suppressed Oxidation and Photodarkening of Hybrid Tin Iodide Perovskite Achieved with Reductive Organic Small Molecule

Jue Gong[#], Xun Li[#], Wei Huang, Peijun Guo, Tobin J. Marks, Richard D. Schaller, and Tao Xu^{*}



Cite This: ACS Appl. Energy Mater. 2021, 4, 4704–4710



Read Online

ACCESS |

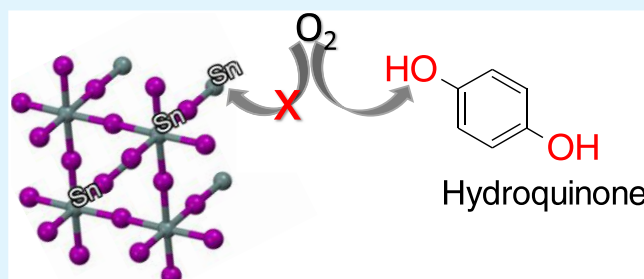
Metrics & More

Article Recommendations

Supporting Information

ABSTRACT: Tin(II)-based halide perovskites have shown promise in lead-free and mixed tin(II)–lead ideal-band-gap photovoltaic applications. Nonetheless, they notoriously suffer from oxidation in oxygen environments, thereby sustaining rapid self-doping during synthesis and further material degradation in postfabrication stages. As such, enhancing the chemical stabilities of tin(II) halide perovskites is imperatively crucial for the further advancement of any relevant eco-friendly and low-band-gap photovoltaic technology. Here, we demonstrate that hydroquinone, a chemically reductive organic molecule, can effectively improve the stability of perovskite methylammonium tin(II) iodide ($\text{CH}_3\text{NH}_3\text{SnI}_3$) in a dry air environment, as shown by X-ray diffraction and X-ray photoelectron spectroscopic studies. Furthermore, the luminescence longevity of the hydroquinone-treated $\text{CH}_3\text{NH}_3\text{SnI}_3$ film is much greater than its undoped pristine counterpart in ambient air, as unambiguously evidenced by their time-dependent steady-state photoluminescence spectra. Meanwhile, time-resolved photoluminescence (TR-PL) decays reveal nearly unchanged carrier recombination lifetimes in both types of perovskite materials during degradation, which therefore infers a facile oxidation process for these thin films. This work provides a practical clue to stable and high-performance tin(II)-based perovskite optoelectronics.

KEYWORDS: halide perovskite, lead-free, photoluminescence, oxidation, hydroquinone



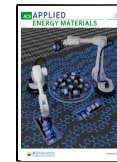
Halide perovskites have realized remarkable performance in optoelectronic applications, such as photovoltaics,^{1–5} photodetectors,^{6,7} and nanolasers,^{8,9} where a certified record power conversion efficiency exceeding 25% has been impressively achieved from perovskite solar cells in 2019.¹⁰ Nonetheless, the majority of the abovementioned high-performing optoelectronics were fabricated on perovskites with lead-based compositions (chemical formula: APbX_3 , $\text{A} = \text{CH}_3\text{NH}_3^+$ (MA^+), $\text{HC}(\text{NH}_2)_2^+$, Cs^+ , $\text{X} = \text{I}^-$, Br^- , and/or Cl^-), in which Pb is highly toxic and detrimental to the environment^{11–15} and thus hinders large-scale commercialization^{16–19} of any relevant energy technologies. Therefore, it is of imperative imminence to substitute Pb with less-toxic elements in perovskites as the light-harvesting active materials. Previous examples of Pb-free perovskites include the adoption of Bi^{3+} or $\text{Bi}^{3+}/\text{Ag}^+$ as B-site cations.^{20–24} However, such practices inevitably result in quasi zero-dimensional structures as in $(\text{CH}_3\text{NH}_3)_3\text{Bi}_2\text{I}_9$ and $\text{Cs}_3\text{Bi}_2\text{I}_9$,^{25,26} or double-perovskite systems (e.g., $\text{Cs}_2\text{BiAgBr}_6$, $\text{Cs}_2\text{BiAgCl}_6$) with indirect band gaps,^{22,27,28} thereby significantly limiting the charge generation and transports therein. Being a group 4A element, Sn has demonstrated its potential in Pb-free solar cells^{12,29–32} and photodetectors³³ with considerable optoelectronic performance. Additionally, the incorporation of Sn in perovskite systems also synergistically brings forth much smaller optical band gaps and greater carrier mobilities due to the more covalent nature of Sn relative to

Pb ^{34–39} thus signifying the capability in further approaching the Shockley–Queisser limit.^{40–42} Nevertheless, tin(II)-based perovskites are plagued by Sn-vacancy defect formation, thus rendering inferior charge carrier properties.^{43–45} Most importantly, Sn^{2+} is easily oxidized to Sn^{4+} in ambient atmosphere^{46,47} and even environments with trace oxygen (<10 ppm) such as a glovebox^{46,48} or precursor solution,⁴⁹ causing the corresponding material processing conditions/windows to be harsh and narrow. Furthermore, oxidation of Sn^{2+} leads to heavily p-doped perovskites⁵⁰ (a process called self-doping), thus deteriorating the final semiconducting properties and photovoltaic performance of solar cell devices. As such, it is intriguing at both technological and scientific levels to enhance the chemical stabilities of Sn(II)-based perovskite materials, so as to further mature the environmental friendly and low-band-gap optoelectronics in the setting of commercial deployment with advanced performance. Herein, we show that through adding a type of reductive organic molecule—hydroquinone

Received: January 29, 2021

Accepted: April 9, 2021

Published: April 22, 2021



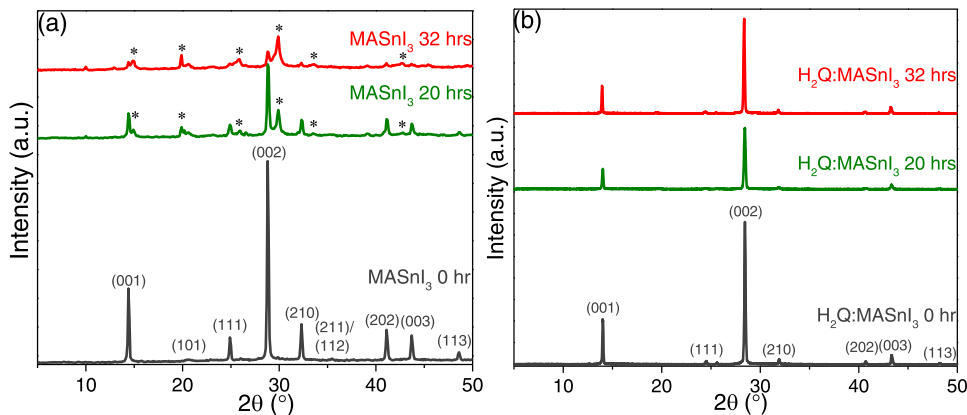


Figure 1. Time-dependent X-ray diffraction patterns of pristine MASnI_3 (a) and 3% w/w H_2Q -doped MASnI_3 (b) thin films in dry air ($\text{RH} < 5\%$). * indicates degradation products.

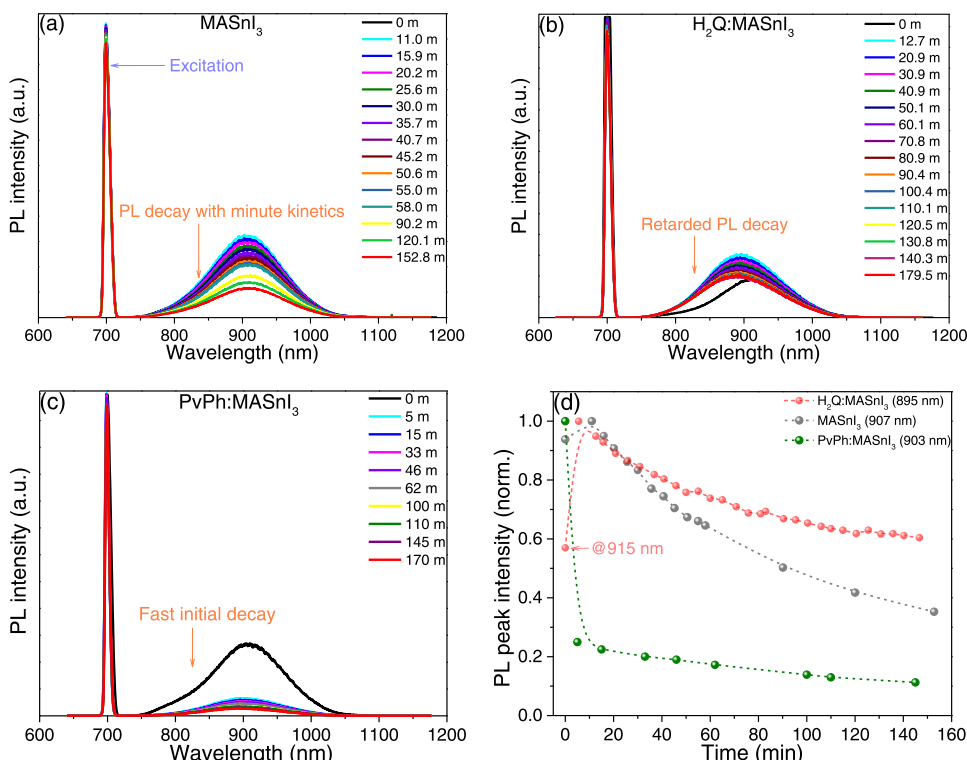


Figure 2. Photodarkening of MASnI_3 with and without organic additives. Evolution of time-integrated PL spectra over time for pristine MASnI_3 (a), 3% w/w H_2Q -doped MASnI_3 (b), and 5% v/v PvPh -doped MASnI_3 (c) thin films. (d) Summary and comparison of PL peak intensities of the three types of tin(II) perovskite thin-film samples, where the dashed lines serve as guides to the eye for the evolution of PL intensities.

(chemical formula: $\text{C}_6\text{H}_4(\text{OH})_2$, denoted H_2Q) with a notably higher oxidation potential than Sn^{2+} in the precursor solution of the perovskite $\text{CH}_3\text{NH}_3\text{SnI}_3$ (MASnI_3), as-fabricated MASnI_3 films exhibit greatly retarded degradation in a dry air environment when compared with the untreated MASnI_3 counterpart. Accordingly, X-ray photoelectron spectra (XPS) reveal a much slower surface oxidation of Sn^{2+} to Sn^{4+} in the presence of H_2Q . Moreover, the improved chemical stability of MASnI_3 leads to a concomitantly enhanced photoluminescence (PL) stability in ambient air under continuous illumination of excitation light, as shown by time-dependent PL spectra. Such suppressed PL photodarkening is optically addressable in tin(II)-based perovskite light-emitting applications with improved operational stabilities.⁵¹ Our work does not introduce excess Sn^{2+} or a highly reducing gaseous environment,^{46,47}

thereby rendering a technically and cost feasible route to stabilizing the Sn(II)-based halide perovskites during both synthesis and postsynthesis stages, and will largely contribute to the continual development of this class of lead-free materials for wide-range energy applications.

To illustrate the stabilizing effects of H_2Q on the perovskite MASnI_3 , we first fabricate pristine and H_2Q -doped MASnI_3 thin films by adding H_2Q (3 wt % content) into the perovskite precursor solution (see the Supporting Information for details). XRD studies confirm the α -phase perovskite structure for both types of MASnI_3 films according to previous reports,^{12,52} as shown by the diffraction patterns in black color of Figure 1. While the addition of H_2Q does not change the perovskite structure of MASnI_3 , it is noticeable to see that the as-fabricated $\text{H}_2\text{Q}:\text{MASnI}_3$ film possesses greater lattice strain than the

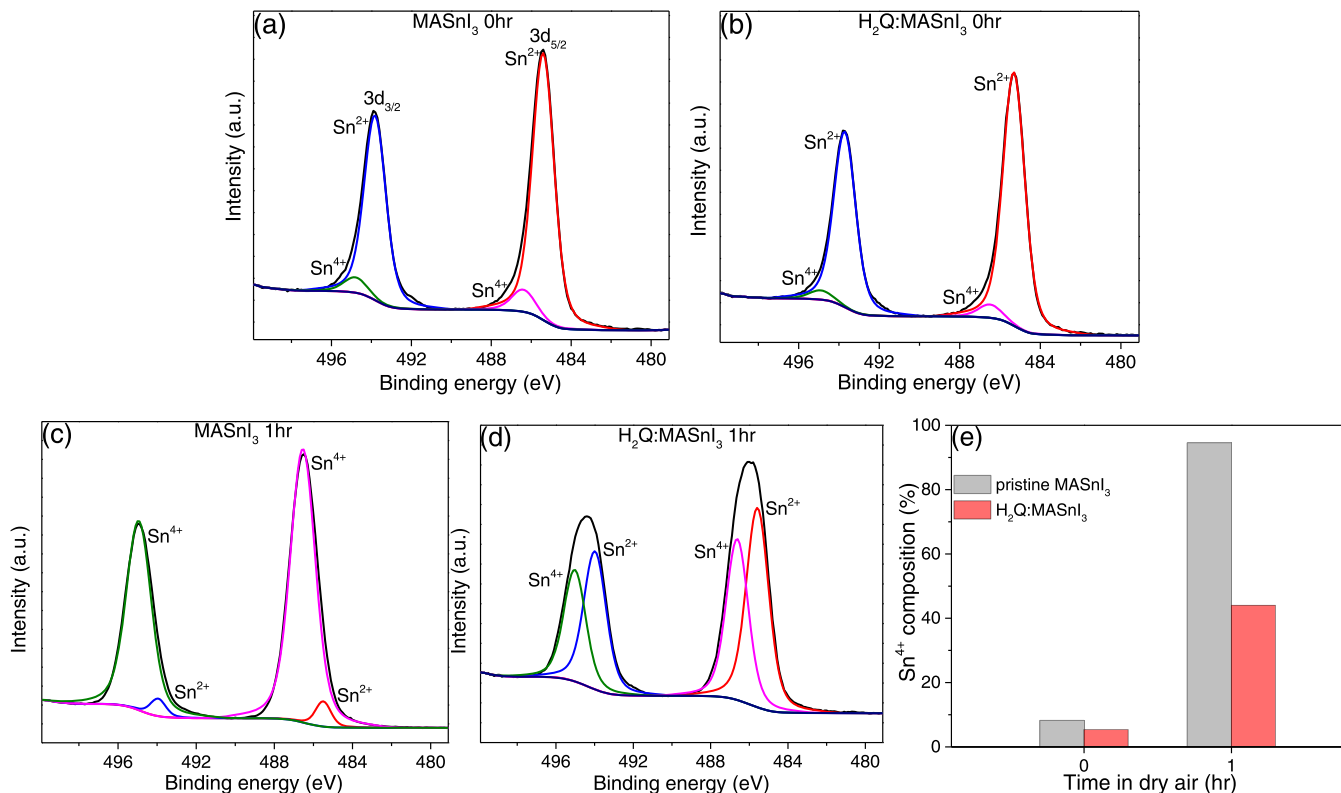


Figure 3. XPS Sn 3d spectra of MASnI₃ (a, c) and H₂Q:MASnI₃ (b, d) measured after aging in dry air for 0 and 1 h, respectively. (e) Comparison of Sn⁴⁺ content in pristine MASnI₃ and H₂Q-doped MASnI₃ before and after 1 h oxidation in dry air.

pristine counterpart, as shown in Figure S1, where lattice strain has been regarded as being closely related to the detailed chemical compositions of tin(II)-based perovskites.⁵³ Therefore, the increased lattice strain can phenomenologically signify the inclusion of H₂Q within the MASnI₃ lattice. Intuitively, infrared spectroscopy confirms the existence of H₂Q in MASnI₃ by showing C–O stretching mode at around 1211 cm⁻¹, in-plane and out-of-plane O–H bending modes at around 1412 and 756 cm⁻¹, respectively, as shown in Figure S2. From the standpoint of optical absorption, the inclusion of H₂Q in MASnI₃ leads to a slightly widened band gap from 1.32 to 1.38 eV, as shown in Figure S3. Most importantly, by aging in dry air with relative humidity (RH) <5% for 20–32 h, the pristine MASnI₃ film clearly shows the appearance of degradation products that are coexistent with the original perovskite phase (Figure 1a); in the meantime, H₂Q:MASnI₃ is free of any degradation phases and only sustains a slight decrease in the peak intensities along the (001) and (002) lattice orientations (Figure 1b). To elucidate the degradation products in pristine MASnI₃, we performed Rietveld refinement on the XRD pattern of the material after 48 h of aging in dry air, where the material is almost completely degraded. As shown in Figure S4, the XRD pattern of significantly degraded “MASnI₃” matches well with (MA)₂SnI₆, a Sn⁴⁺ structural variant, thus confirming the degradation of MASnI₃ being Sn²⁺ oxidation. The formation of oxidized products in air agrees well with previous reports on tin(II)-based perovskites.⁵⁴ Importantly, to rule out the physical and morphological factors that could also affect the chemical stability against oxidation of both types of perovskite thin films, we then performed scanning electron microscopy (SEM) on the surface of both film samples. As shown in Figure S5, both films have comparable surface morphology with densely covered

grains, thereby ruling out the potential physical effects of perovskite samples and suggesting that H₂Q is indeed the chemical origin that suppressed the observed oxidation of MASnI₃.

Since photoluminescence (PL) is a physical property that is sensitive to the chemical and structural changes of crystalline materials,^{55,56} we subsequently performed steady-state PL spectroscopy on the tin(II)-based perovskites under continuous 700 nm optical excitation to examine their stabilities in an ambient air condition. As shown in Figure 2a,d, pristine MASnI₃ thin film exhibits PL emissions, whose peak intensities (at 907 nm) decrease in minutes. Noteworthily, this minute-kinetic decay starts with a maximum PL intensity at around 11 min after the material was exposed to air and is preceded by an initial PL with slightly less intensity (~0.94 of the maximum intensity) as measured immediately upon air exposure (Figure 2a,d). Such rise and decay of PL intensities are attributed to photoinduced activation and darkening processes,^{57–59} which are, respectively, related to the defect passivation by illumination in the presence of H₂O/O₂ and material degradation in air.^{57,60,61} By contrast, the H₂Q-containing MASnI₃ thin film demonstrates a profoundly retarded PL decay, where a more pronounced initial photoactivation—from 0.57 at 0 min to maximum intensity at ~12.7 min of air exposure, and a blue shift of PL center wavelength from 915 to 895 nm are observed (Figure 2b,d), which is attributable to halide redistribution in the presence of organic additive H₂Q as similarly reported in previous reports.^{59,62} On the other hand, the more obvious photoactivation of H₂Q:MASnI₃ after exposure to air suggests that the nonradiative defects were not originally passivated by H₂Q upon doping, but the subsequent photodarkening process owing to chemical change of perovskite material is greatly mitigated.⁶³

Meanwhile, the blue-shifted PL center wavelength of $\text{H}_2\text{Q}:\text{MASnI}_3$ with respect to pristine MASnI_3 agrees well with its larger optical band gap extracted from UV-vis absorbance studies in Figure S3. Such phenomena altogether indicate that H_2Q is indeed doped into MASnI_3 and has effectively slowed the material degradation while also changing the luminescence behavior of MASnI_3 upon its exposure to ambient air. Although pristine MASnI_3 and $\text{H}_2\text{Q}:\text{MASnI}_3$ exhibit decreases in PL intensity in air, we surprisingly find that their charge recombination lifetimes maintain relatively constant during the air degradation processes except for a long-component lifetime (τ_2) increase on $\text{H}_2\text{Q}:\text{MASnI}_3$ after initial air exposure, which again points to the effects of H_2Q on the defect properties of MASnI_3 perovskite in the presence of air molecules, as shown in Figure S6e,f. The largely unaffected charge recombination lifetimes after initial air exposure imply that the degradation of MASnI_3 thin films adopts a rapid and facile manner, where the nonluminescence degradation products only contribute to the continuously reduced transient PL peak intensity (Figure S6a,c) but not to the intrinsic Sn-vacancy concentration that is directly related to carrier lifetime.^{46,64} However, it should be noted that τ_2 of pristine MASnI_3 (~3.3 ns) as measured at 0 h of air exposure is notably longer than $\text{H}_2\text{Q}:\text{MASnI}_3$ (~1.4 ns), which potentially implies a negative impact on the photovoltaic performance of encapsulated solar cell devices that avoid air exposure.

At this point, it is logical to consider the mechanistic origin of the antioxidant effects of H_2Q on perovskite MASnI_3 . From an organic chemistry standpoint, the secondary hydroxyl ($-\text{OH}$) groups in H_2Q could be the entity responsible for the improved stability, as $-\text{OH}$ is oxidized through dehydrogenation reaction to become ketone ($\text{C}=\text{O}$), thereby sacrificially suppressing the oxidation of Sn^{2+} to Sn^{4+} and thus the photodarkening of MASnI_3 . Nevertheless, we discovered that not all OH^- -containing organic molecules are capable of extending the PL lifetime of perovskite MASnI_3 , exemplified by a 5% v/v PvPh-doped MASnI_3 film (PvPh: poly(4-vinylphenol), see the Supporting Information for details) that shows ~75% reduction in PL intensity after only 5 min of exposure to air, as shown in Figure 2c,d. This observation suggests the necessity of screening both the chemical functional group and molecular structure in designing effective dopants for stabilizing tin(II)-based perovskites.

To further substantiate the effectiveness and the mechanistic root cause of H_2Q in the suppressed MASnI_3 degradation, we subsequently conducted X-ray photoelectron spectroscopy (XPS) on pristine MASnI_3 and $\text{H}_2\text{Q}:\text{MASnI}_3$ films. As shown in Figure 3a,b,e, MASnI_3 and $\text{H}_2\text{Q}:\text{MASnI}_3$ films at 0 h of air exposure have mostly the Sn^{2+} compositions but inevitably contain Sn^{4+} (8.25% for pristine MASnI_3 , 5.36% for $\text{H}_2\text{Q}:\text{MASnI}_3$, see Tables S1 and S2 for determination of atomic compositions of $\text{Sn}^{4+}/\text{Sn}^{2+}$), which is due to the rapid surface oxidation during the sample transfer into the XPS chamber and was likewise observed in a previous report of tin(II)-based perovskites.⁴⁶ Nevertheless, after 1 h of aging in dry air ($\text{RH} < 5\%$), it is clear that the Sn^{4+} content of pristine MASnI_3 rises to 94.6%, while Sn^{4+} concentration in $\text{H}_2\text{Q}:\text{MASnI}_3$ only increases to 44.0% (see Tables S3 and S4 for determination of atomic compositions of $\text{Sn}^{4+}/\text{Sn}^{2+}$), as shown in Figure 3c–e. The large difference in Sn^{4+} generation thus confirms the antioxidant function of H_2Q toward perovskite MASnI_3 .

From the electrochemistry perspective, full oxidation of Sn^{2+} in perovskites typically requires the joint effects of water and

oxygen.^{65,66} As a consequence, redox reaction potentials of Sn species and H_2Q can be compared to reveal the working mechanism of H_2Q in suppressing the oxidation of Sn^{2+} in MASnI_3 . As shown in Figure 4, based on the standard potentials

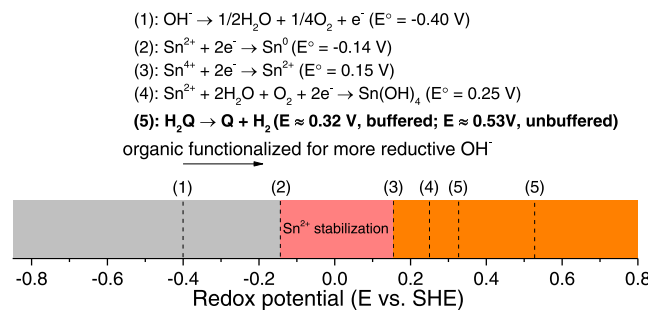


Figure 4. Scheme of redox reactions related to Sn chemical species and H_2Q . Based on the half-reaction potentials of OH^- oxidation and $\text{Sn}^{2+}/\text{Sn}^{4+}$ reduction, oxidation of H_2Q is the most spontaneous, with its oxidation potentials taken from ref 67.

(referenced to a standard hydrogen electrode (SHE)) of Sn^{4+} reduction and OH^- oxidation (half-reactions 1 and 3), one can deduce the oxidation potential of Sn^{2+} reaction with both water and oxygen, which possesses a 0.25 V potential (vs SHE, full reaction 4). Such reaction potential is apparently smaller than the oxidation potential of H_2Q —0.32 V vs SHE at 25 °C pH = 7 buffered condition, and 0.53 V vs SHE in an unbuffered environment (see the Supporting Information for detailed analysis) as per previous electrochemical studies,⁶⁷ thereby making the oxidation of H_2Q more spontaneous than Sn^{2+} , or in other words, an effective reducing agent for preserving Sn^{2+} in MASnI_3 . The reducing effects of H_2Q can also be rationalized from the fact that sp^2 -hybridized C atom and OH share electrons due to the covalent bond, thus rendering the bonded electrons easier to lose than individual OH^- ions (half-reaction 1).

In summary, we proved that the doping of a reductive organic molecule, hydroquinone, into the perovskite MASnI_3 , can enable greatly suppressed material degradation and photodarkening in air conditions, as manifested in time-dependent XRD and steady-state PL studies. The retarded material degradation and prolonged PL retention rely on the foundation where Sn^{2+} oxidation is suppressed, which is realized through the more spontaneous oxidation of hydroquinone as verified by XPS and electrochemical analysis. Our work helps to further develop lead-free perovskite optoelectronics with enhanced stabilities for scale-up and higher-performance applications.

ASSOCIATED CONTENT

Supporting Information

The Supporting Information is available free of charge at <https://pubs.acs.org/doi/10.1021/acsaem.1c00316>.

Experimental methods for material preparation and characterizations; Williamson–Hall plots (Figure S1); Fourier transform infrared spectra of pristine MASnI_3 (gray) and $\text{H}_2\text{Q}:\text{MASnI}_3$ (red) films (Figure S2); UV-vis absorbance spectra of $\text{H}_2\text{Q}:\text{MASnI}_3$ (red) and pristine MASnI_3 (gray) films (Figure S3); XRD refinement of MASnI_3 film (Figure S4); scanning electron microscopic images (Figure S5); time-resolved photoluminescence (Figure S6); peak fitting of Sn 3d photoelectrons of pristine MASnI_3 with 0 h of exposure (Table S1); peak fitting of Sn 3d photoelectrons of pristine MASnI_3 with 1

h of exposure (Table S2); peak fitting of Sn 3d photoelectrons of $H_2Q:MASnI_3$ with 0 h of exposure (Table S3); and peak fitting of Sn 3d photoelectrons of $H_2Q:MASnI_3$ with 1 h of exposure (Table S4) ([PDF](#))

AUTHOR INFORMATION

Corresponding Author

Tao Xu — Department of Chemistry and Biochemistry, Northern Illinois University, DeKalb, Illinois 60115, United States; [orcid.org/0000-0002-3343-7263](#); Email: txu@niu.edu

Authors

Jue Gong — Department of Chemistry and Biochemistry, Northern Illinois University, DeKalb, Illinois 60115, United States

Xun Li — Department of Chemistry and Biochemistry, Northern Illinois University, DeKalb, Illinois 60115, United States

Wei Huang — Department of Chemistry and Materials Research Center, Northwestern University, Evanston, Illinois 60208, United States; [orcid.org/0000-0002-0973-8015](#)

Peijun Guo — Department of Chemical and Environmental Engineering, Yale University, New Haven, Connecticut 06520, United States; [orcid.org/0000-0001-5732-7061](#)

Tobin J. Marks — Department of Chemistry and Materials Research Center, Northwestern University, Evanston, Illinois 60208, United States; [orcid.org/0000-0001-8771-0141](#)

Richard D. Schaller — Department of Chemistry, Northwestern University, Evanston, Illinois 60208, United States; Center for Nanoscale Materials, Argonne National Laboratory, Argonne, Illinois 60439, United States; [orcid.org/0000-0001-9696-8830](#)

Complete contact information is available at:
<https://pubs.acs.org/10.1021/acsaem.1c00316>

Author Contributions

#J.G. and X.L. contributed equally to this work.

Notes

The authors declare no competing financial interest.

ACKNOWLEDGMENTS

J.G., X.L., and T.X. acknowledge the funding support from the US National Science Foundation (DMR-1806152). This work was performed, in part, at the Center for Nanoscale Materials, a U.S. Department of Energy Office of Science User Facility, and supported by the U.S. Department of Energy, Office of Science, under Contract No. DE-AC02-06CH11357. W.H. and T.J.M. acknowledge support from Northwestern University National Science Foundation MRSEC (DMR-1720139).

REFERENCES

- (1) Jiang, Q.; Zhao, Y.; Zhang, X.; Yang, X.; Chen, Y.; Chu, Z.; Ye, Q.; Li, X.; Yin, Z.; You, J. Surface Passivation of Perovskite Film for Efficient Solar Cells. *Nat. Photonics* **2019**, *13*, 460–466.
- (2) Nie, W.; Tsai, H.; Asadpour, R.; Blancon, J.-C.; Neukirch, A. J.; Gupta, G.; Crochet, J. J.; Chhowalla, M.; Tretiak, S.; Alam, M. A.; Wang, H.-L.; Mohite, A. D. High-Efficiency Solution-Processed Perovskite Solar Cells with Millimeter-Scale Grains. *Science* **2015**, *347*, 522–525.
- (3) Yang, W. S.; Noh, J. H.; Jeon, N. J.; Kim, Y. C.; Ryu, S.; Seo, J.; Seok, S. I. High-Performance Photovoltaic Perovskite Layers Fabricated through Intramolecular Exchange. *Science* **2015**, *348*, 1234–1237.

(4) Yang, W. S.; Park, B.-W.; Jung, E. H.; Jeon, N. J.; Kim, Y. C.; Lee, D. U.; Shin, S. S.; Seo, J.; Kim, E. K.; Noh, J. H.; Seok, S. I. Iodide Management in Formamidinium-Lead-Halide-based Perovskite Layers for Efficient Solar Cells. *Science* **2017**, *356*, 1376–1379.

(5) Chen, W.; Wu, Y.; Yue, Y.; Liu, J.; Zhang, W.; Yang, X.; Chen, H.; Bi, E.; Ashraful, I.; Grätzel, M.; Han, L. Efficient and Stable Large-Area Perovskite Solar Cells with Inorganic Charge Extraction Layers. *Science* **2015**, *350*, 944–948.

(6) Dou, L.; Yang, Y. M.; You, J.; Hong, Z.; Chang, W.-H.; Li, G.; Yang, Y. Solution-Processed Hybrid Perovskite Photodetectors with High Detectivity. *Nat. Commun.* **2014**, *5*, No. 5404.

(7) Shrestha, S.; Fischer, R.; Matt, G. J.; Feldner, P.; Michel, T.; Osvet, A.; Levchuk, I.; Merle, B.; Golkar, S.; Chen, H.; Tedde, S. F.; Schmidt, O.; Hock, R.; Rührig, M.; Göken, M.; Heiss, W.; Anton, G.; Brabec, C. J. High-Performance Direct Conversion X-ray Detectors based on Sintered Hybrid Lead Triiodide Perovskite Wafers. *Nat. Photonics* **2017**, *11*, 436–440.

(8) Zhu, H.; Fu, Y.; Meng, F.; Wu, X.; Gong, Z.; Ding, Q.; Gustafsson, M. V.; Trinh, M. T.; Jin, S.; Zhu, X.-Y. Lead Halide Perovskite Nanowire Lasers with Low Lasing Thresholds and High Quality Factors. *Nat. Mater.* **2015**, *14*, 636–642.

(9) Fu, Y.; Zhu, H.; Schrader, A. W.; Liang, D.; Ding, Q.; Joshi, P.; Hwang, L.; Zhu, X.-Y.; Jin, S. Nanowire Lasers of Formamidinium Lead Halide Perovskites and Their Stabilized Alloys with Improved Stability. *Nano Lett.* **2016**, *16*, 1000–1008.

(10) National Renewable Energy Laboratory Best Research-Cell Efficiencies, NREL Research Cell Efficiency Records; National Renewable Energy Laboratory: Golden, CO, 2021. <https://www.nrel.gov/pv/assets/pdfs/best-research-cell-efficiencies.20190802.pdf> (accessed April 8, 2021).

(11) Li, X.; Zhang, F.; He, H.; Berry, J. J.; Zhu, K.; Xu, T. On-Device Lead Sequestration for Perovskite Solar Cells. *Nature* **2020**, *578*, 555–558.

(12) Hao, F.; Stoumpos, C. C.; Cao, D. H.; Chang, R. P. H.; Kanatzidis, M. G. Lead-Free Solid-State Organic-Inorganic Halide Perovskite Solar Cells. *Nat. Photonics* **2014**, *8*, 489–494.

(13) Shi, Z.; Guo, J.; Chen, Y.; Li, Q.; Pan, Y.; Zhang, H.; Xia, Y.; Huang, W. Lead-Free Organic-Inorganic Hybrid Perovskites for Photovoltaic Applications: Recent Advances and Perspectives. *Adv. Mater.* **2017**, *29*, No. 1605005.

(14) Abate, A. Perovskite Solar Cells Go Lead Free. *Joule* **2017**, *1*, 659–664.

(15) Grätzel, M. The Light and Shade of Perovskite Solar Cells. *Nat. Mater.* **2014**, *13*, 838–842.

(16) Green, M. A.; Ho-Baillie, A.; Snaith, H. J. The Emergence of Perovskite Solar Cells. *Nat. Photonics* **2014**, *8*, 506–514.

(17) Jiang, Y.; Qiu, L.; Juarez-Perez, E. J.; Ono, L. K.; Hu, Z.; Liu, Z.; Wu, Z.; Meng, L.; Wang, Q.; Qi, Y. Reduction of Lead Leakage from Damaged Lead Halide Perovskite Solar Modules Using Self-Healing Polymer-based Encapsulation. *Nat. Energy* **2019**, *4*, 585–593.

(18) Ke, W.; Kanatzidis, M. G. Prospects for Low-Toxicity Lead-Free Perovskite Solar Cells. *Nat. Commun.* **2019**, *10*, No. 965.

(19) Chen, M.; Ju, M.-G.; Garces, H. F.; Carl, A. D.; Ono, L. K.; Hawash, Z.; Zhang, Y.; Shen, T.; Qi, Y.; Grimm, R. L.; Pacifici, D.; Zeng, X. C.; Zhou, Y.; Padture, N. P. Highly Stable and Efficient All-Inorganic Lead-Free Perovskite Solar Cells with Native-Oxide Passivation. *Nat. Commun.* **2019**, *10*, No. 16.

(20) Park, B.-W.; Philippe, B.; Zhang, X.; Rensmo, H.; Boschloo, G.; Johansson, E. M. J. Bismuth Based Hybrid Perovskites $A_3Bi_2I_9$ (A: Methylammonium or Cesium) for Solar Cell Application. *Adv. Mater.* **2015**, *27*, 6806–6813.

(21) Zhang, Z.; Li, X.; Xia, X.; Wang, Z.; Huang, Z.; Lei, B.; Gao, Y. High-Quality $(CH_3NH_3)_3Bi_2I_9$ Film-Based Solar Cells: Pushing Efficiency up to 1.64%. *J. Phys. Chem. Lett.* **2017**, *8*, 4300–4307.

(22) Slavney, A. H.; Hu, T.; Lindenberg, A. M.; Karunadasa, H. I. A Bismuth-Halide Double Perovskite with Long Carrier Recombination Lifetime for Photovoltaic Applications. *J. Am. Chem. Soc.* **2016**, *138*, 2138–2141.

- (23) McClure, E. T.; Ball, M. R.; Windl, W.; Woodward, P. M. $\text{Cs}_2\text{AgBiX}_6$ ($X = \text{Br}, \text{Cl}$): New Visible Light Absorbing, Lead-Free Halide Perovskite Semiconductors. *Chem. Mater.* **2016**, *28*, 1348–1354.
- (24) Slavney, A. H.; Smaha, R. W.; Smith, I. C.; Jaffe, A.; Umeyama, D.; Karunadasa, H. I. Chemical Approaches to Addressing the Instability and Toxicity of Lead-Halide Perovskite Absorbers. *Inorg. Chem.* **2017**, *56*, 46–55.
- (25) McCall, K. M.; Stoumpos, C. C.; Kontsevoi, O. Y.; Alexander, G. C. B.; Wessels, B. W.; Kanatzidis, M. G. From 0D $\text{Cs}_3\text{Bi}_2\text{I}_9$ to 2D $\text{Cs}_3\text{Bi}_2\text{I}_6\text{Cl}_3$: Dimensional Expansion Induces a Direct Band Gap but Enhances Electron-Phonon Coupling. *Chem. Mater.* **2019**, *31*, 2644–2650.
- (26) Ni, C.; Hedley, G.; Payne, J.; Svrcek, V.; McDonald, C.; Jagadamma, L. K.; Edwards, P.; Martin, R.; Jain, G.; Carolan, D.; Mariotti, D.; Maguire, P.; Samuel, I.; Irvine, J. Charge Carrier Localised in Zero-Dimensional $(\text{CH}_3\text{NH}_3)_3\text{Bi}_2\text{I}_9$ Clusters. *Nat. Commun.* **2017**, *8*, No. 170.
- (27) Slavney, A. H.; Leppert, L.; Bartesaghi, D.; Gold-Parker, A.; Toney, M. F.; Savenije, T. J.; Neaton, J. B.; Karunadasa, H. I. Defect-Induced Band-Edge Reconstruction of a Bismuth-Halide Double Perovskite for Visible-Light Absorption. *J. Am. Chem. Soc.* **2017**, *139*, 5015–5018.
- (28) Savory, C. N.; Walsh, A.; Scanlon, D. O. Can Pb-Free Halide Double Perovskites Support High-Efficiency Solar Cells? *ACS Energy Lett.* **2016**, *1*, 949–955.
- (29) Hao, F.; Stoumpos, C. C.; Guo, P.; Zhou, N.; Marks, T. J.; Chang, R. P. H.; Kanatzidis, M. G. Solvent-Mediated Crystallization of $\text{CH}_3\text{NH}_3\text{SnI}_3$ Films for Heterojunction Depleted Perovskite Solar Cells. *J. Am. Chem. Soc.* **2015**, *137*, 11445–11452.
- (30) Hao, F.; Stoumpos, C. C.; Chang, R. P. H.; Kanatzidis, M. G. Anomalous Band Gap Behavior in Mixed Sn and Pb Perovskites Enables Broadening of Absorption Spectrum in Solar Cells. *J. Am. Chem. Soc.* **2014**, *136*, 8094–8099.
- (31) Noel, N. K.; Stranks, S. D.; Abate, A.; Wehrenfennig, C.; Guarnera, S.; Haghhighirad, A.-A.; Sadhanala, A.; Eperon, G. E.; Pathak, S. K.; Johnston, M. B.; Petrozza, A.; Herz, L. M.; Snaith, H. J. Lead-Free Organic-Inorganic Tin Halide Perovskites for Photovoltaic Applications. *Energy Environ. Sci.* **2014**, *7*, 3061–3068.
- (32) Shao, S.; Liu, J.; Portale, G.; Fang, H.-H.; Blake, G. R.; ten Brink, G. H.; Koster, L. J. A.; Loi, M. A. Highly Reproducible Sn-Based Hybrid Perovskite Solar Cells with 9% Efficiency. *Adv. Energy Mater.* **2018**, *8*, No. 1702019.
- (33) Liu, C.-K.; Tai, Q.; Wang, N.; Tang, G.; Loi, H.-L.; Yan, F. Sn-Based Perovskite for Highly Sensitive Photodetectors. *Adv. Sci.* **2019**, *6*, No. 1900751.
- (34) Zong, Y.; Zhou, Z.; Chen, M.; Padture, N. P.; Zhou, Y. Lewis-Adduct Mediated Grain-Boundary Functionalization for Efficient Ideal-Bandgap Perovskite Solar Cells with Superior Stability. *Adv. Energy Mater.* **2018**, *8*, No. 1800997.
- (35) Zong, Y.; Wang, N.; Zhang, L.; Ju, M.-G.; Zeng, X. C.; Sun, X. W.; Zhou, Y.; Padture, N. P. Homogenous Alloys of Formamidinium Lead Triiodide and Cesium Tin Triiodide for Efficient Ideal-Bandgap Perovskite Solar Cells. *Angew. Chem., Int. Ed.* **2017**, *56*, 12658–12662.
- (36) Wu, B.; Zhou, Y.; Xing, G.; Xu, Q.; Garces, H. F.; Solanki, A.; Goh, T. W.; Padture, N. P.; Sum, T. C. Long Minority-Carrier Diffusion Length and Low Surface-Recombination Velocity in Inorganic Lead-Free CsSnI_3 Perovskite Crystal for Solar Cells. *Adv. Funct. Mater.* **2017**, *27*, No. 1604818.
- (37) Wang, N.; Zhou, Y.; Ju, M.-G.; Garces, H. F.; Ding, T.; Pang, S.; Zeng, X. C.; Padture, N. P.; Sun, X. W. Heterojunction-Depleted Lead-Free Perovskite Solar Cells with Coarse-Grained $\text{B}-\gamma\text{-CsSnI}_3$ Thin Films. *Adv. Energy Mater.* **2016**, *6*, No. 1601130.
- (38) Gong, J.; Yang, M.; Rebollar, D.; Rucinski, J.; Liveris, Z.; Zhu, K.; Xu, T. Divalent Anionic Doping in Perovskite Solar Cells for Enhanced Chemical Stability. *Adv. Mater.* **2018**, *30*, No. 1800973.
- (39) Herz, L. M. Charge-Carrier Mobilities in Metal Halide Perovskites: Fundamental Mechanisms and Limits. *ACS Energy Lett.* **2017**, *2*, 1539–1548.
- (40) Shockley, W.; Queisser, H. J. Detailed Balance Limit of Efficiency of $p-n$ Junction Solar Cells. *J. Appl. Phys.* **1961**, *32*, 510.
- (41) Kong, L.; Liu, G.; Gong, J.; Hu, Q.; Schaller, R. D.; Dera, P.; Zhang, D.; Liu, Z.; Yang, W.; Zhu, K.; Tang, Y.; Wang, C.; Wei, S.-H.; Mao, H.-k.; et al. Simultaneous Band-Gap Narrowing and Carrier-Lifetime Prolongation of Organic-Inorganic Trihalide Perovskites. *Proc. Natl. Acad. Sci. U.S.A.* **2016**, *113*, 8910–8915.
- (42) Liu, G.; Kong, L.; Gong, J.; Yang, W.; Mao, H.-k.; Hu, Q.; Liu, Z.; Schaller, R. D.; Zhang, D.; Xu, T. Pressure-Induced Bandgap Optimization in Lead-Based Perovskites with Prolonged Carrier Lifetime and Ambient Retainability. *Adv. Funct. Mater.* **2017**, *27*, No. 1604208.
- (43) Liu, X.; Wu, T.; Chen, J.-Y.; Meng, X.; He, X.; Noda, T.; Chen, H.; Yang, X.; Segawa, H.; Wang, Y.; Han, L. Tempered Growth of FASnI_3 Crystals for Efficient Tin Perovskite Solar Cells. *Energy Environ. Sci.* **2020**, *13*, 2896–2902.
- (44) Lanzetta, L.; Aristidou, N.; Haque, S. A. Stability of Lead and Tin Halide Perovskites: the Link between Defects and Degradation. *J. Phys. Chem. Lett.* **2020**, *11*, 574–585.
- (45) Luo, X.; Wu, T.; Wang, Y.; Lin, X.; Su, H.; Han, Q.; Han, L. Progress of All-Perovskite Tandem Solar Cells: the Role of Narrow-Bandgap Absorbers. *Sci. China: Chem.* **2021**, *64*, 218–227.
- (46) Song, T.-B.; Yokoyama, T.; Stoumpos, C. C.; Logsdon, J.; Cao, D. H.; Wasielewski, M. R.; Aramaki, S.; Kanatzidis, M. G. Importance of Reducing Vapor Atmosphere in the Fabrication of Tin-Based Perovskite Solar Cells. *J. Am. Chem. Soc.* **2017**, *139*, 836–842.
- (47) Tai, Q.; Guo, X.; Tang, G.; You, P.; Ng, T.-W.; Shen, D.; Cao, J.; Liu, C.-K.; Wang, N.; Zhu, Y.; Lee, C.-S.; Yan, F. Antioxidant Grain Passivation for Air-Stable Tin-Based Perovskite Solar Cells. *Angew. Chem., Int. Ed.* **2019**, *58*, 806–810.
- (48) He, X.; Wu, T.; Liu, X.; Wang, Y.; Meng, X.; Wu, J.; Noda, T.; Yang, X.; Moritomo, Y.; Segawa, H.; Han, L. Highly Efficient Tin Perovskite Solar Cells Achieved in a Wide Oxygen Concentration Range. *J. Mater. Chem. A* **2020**, *8*, 2760–2768.
- (49) Gong, J.; Flatken, M.; Abate, A.; Correa-Baena, J.-P.; Mora-Seró, I.; Saliba, M.; Zhou, Y. The Bloom of Perovskite Optoelectronics: Fundamental Science Matters. *ACS Energy Lett.* **2019**, *4*, 861–865.
- (50) Song, T.-B.; Yokoyama, T.; Logsdon, J.; Wasielewski, M. R.; Aramaki, S.; Kanatzidis, M. G. Piperazine Suppresses Self-Doping in CsSnI_3 Perovskite Solar Cells. *ACS Appl. Energy Mater.* **2018**, *1*, 4221–4226.
- (51) Fan, Q.; Biesold-McGee, G. V.; Ma, J.; Xu, Q.; Pan, S.; Peng, J.; Lin, Z. Lead-Free Halide Perovskite Nanocrystals: Crystal Structures, Synthesis, Stabilities, and Optical Properties. *Angew. Chem., Int. Ed.* **2020**, *59*, 1030–1046.
- (52) Stoumpos, C. C.; Malliakas, C. D.; Kanatzidis, M. G. Semiconducting Tin and Lead Iodide Perovskites with Organic Cations: Phase Transitions, High Mobilities, and Near-Infrared Photoluminescence Properties. *Inorg. Chem.* **2013**, *52*, 9019–9038.
- (53) Kapil, G.; Bessho, T.; Ng, C. H.; Hamada, K.; Pandey, M.; Kamarudin, M. A.; Hirotani, D.; Kinoshita, T.; Minemoto, T.; Shen, Q.; Toyoda, T.; Murakami, T. N.; Segawa, H.; Hayase, S. Strain Relaxation and Light Management in Tin-Lead Perovskite Solar Cells to Achieve High Efficiencies. *ACS Energy Lett.* **2019**, *4*, 1991–1998.
- (54) Qian, F.; Hu, M.; Gong, J.; Ge, C.; Zhou, Y.; Guo, J.; Chen, M.; Ge, Z.; Padture, N. P.; Zhou, Y.; Feng, J. Enhanced Thermoelectric Performance in Lead-Free Inorganic $\text{CsSn}_{1-x}\text{Ge}_x\text{I}_3$ Perovskite Semiconductors. *J. Phys. Chem. C* **2020**, *124*, 11749–11753.
- (55) Guo, P.; Mannodi-Kanakkithodi, A.; Gong, J.; Xia, Y.; Stoumpos, C. C.; Cao, D. H.; Diroll, B. T.; Ketterson, J. B.; Wiederrecht, G. P.; Xu, T.; Chan, M. K. Y.; Kanatzidis, M. G.; Schaller, R. D. Infrared-Pump Electronic-Probe of Methylammonium Lead Iodide Reveals Electronically Decoupled Organic and Inorganic Sublattices. *Nat. Commun.* **2019**, *10*, No. 482.
- (56) Chen, Y.; Lei, Y.; Li, Y.; Yu, Y.; Cai, J.; Chiu, M.-H.; Rao, R.; Gu, Y.; Wang, C.; Choi, W.; Hu, H.; Wang, C.; Li, Y.; Song, J.; Zhang, J.; Qi, B.; Lin, M.; Zhang, Z.; Islam, A. E.; Maruyama, B.; Dayeh, S.; Li, L.-J.; Yang, K.; Lo, Y.-H.; Xu, S. Strain Engineering and Epitaxial Stabilization of Halide Perovskites. *Nature* **2020**, *577*, 209–215.

- (57) Galisteo-López, J. F.; Anaya, M.; Calvo, M. E.; Míguez, H. Environmental Effects on the Photophysics of Organic-Inorganic Halide Perovskites. *J. Phys. Chem. Lett.* **2015**, *6*, 2200–2205.
- (58) Quitsch, W.-A.; deQuilettes, D. W.; Pfingsten, O.; Schmitz, A.; Ognjanovic, S.; Jariwala, S.; Koch, S.; Winterer, M.; Ginger, D. S.; Bacher, G. The Role of Excitation Energy in Photobrightening and Photodegradation of Halide Perovskite Thin Films. *J. Phys. Chem. Lett.* **2018**, *9*, 2062–2069.
- (59) Péan, E. V.; De Castro, C. S.; Davies, M. L. Shining a Light on the Photoluminescence Behaviour of Methylammonium Lead Iodide Perovskite: Investigating the Competing Photobrightening and Photodarkening Processes. *Mater. Lett.* **2019**, *243*, 191–194.
- (60) Fang, H.-H.; Adjokatse, S.; Wei, H.; Yang, J.; Blake, G. R.; Huang, J.; Even, J.; Loi, M. A. Ultrahigh Sensitivity of Methylammonium Lead Tribromide Perovskite Single Crystals to Environmental Gases. *Sci. Adv.* **2016**, *2*, No. e1600534.
- (61) Andaji-Garmaroudi, Z.; Anaya, M.; Pearson, A. J.; Stranks, S. D. Photobrightening in Lead Halide Perovskites: Observations, Mechanisms, and Future Potential. *Adv. Energy Mater.* **2020**, *10*, No. 1903109.
- (62) Cheng, L.; Yi, C.; Tong, Y.; Zhu, L.; Kusch, G.; Wang, X.; Wang, X.; Jiang, T.; Zhang, H.; Zhang, J.; Xue, C.; Chen, H.; Xu, W.; Liu, D.; Oliver, R. A.; Friend, R. H.; Zhang, L.; Wang, N.; Huang, W.; Wang, J. Halide Homogenization for High-Performance Blue Perovskite Electroluminescence. *Research* **2020**, *2020*, No. 9017871.
- (63) Motti, S. G.; Meggiolaro, D.; Barker, A. J.; Mosconi, E.; Perini, C. A. R.; Ball, J. M.; Gandini, M.; Kim, M.; De Angelis, F.; Petrozza, A. Controlling Competing Photochemical Reactions Stabilizes Perovskite Solar Cells. *Nat. Photonics* **2019**, *13*, 532–539.
- (64) Parrott, E. S.; Milot, R. L.; Stergiopoulos, T.; Snaith, H. J.; Johnston, M. B.; Herz, L. M. Effect of Structural Phase Transition on Charge-Carrier Lifetimes and Defects in $\text{CH}_3\text{NH}_3\text{SnI}_3$ Perovskite. *J. Phys. Chem. Lett.* **2016**, *7*, 1321–1326.
- (65) Li, H.; Wei, Q.; Ning, Z. Toward High Efficiency Tin Perovskite Solar Cells: A Perspective. *Appl. Phys. Lett.* **2020**, *117*, No. 060502.
- (66) Xie, G.; Xu, L.; Sun, L.; Xiong, Y.; Wu, P.; Hu, B. Insight into the Reaction Mechanism of Water, Oxygen and Nitrogen Molecules on a Tin Iodine Perovskite Surface. *J. Mater. Chem. A* **2019**, *7*, 5779–5793.
- (67) Rafiee, M.; Nematollahi, D. Voltammetry of Electroinactive Species Using Quinone/Hydroquinone Redox: A Known Redox System Viewed in a New Perspective. *Electroanalysis* **2007**, *19*, 1382–1386.